Variability, timescales, and non-linearity in climate responses to black carbon emissions

Yang Yang[1*], Steven J. Smith[2*], Hailong Wang[1], Catrin M. Mills[1], Philip J. Rasch[1]

[1]Atmospheric Sciences and Global Change Division, Pacific Northwest National Laboratory, Richland, Washington, USA

[2]Joint Global Change Research Institute, Pacific Northwest National Laboratory, College Park, Maryland, USA

*Correspondence to yang.yang@pnnl.gov and ssmith@pnnl.gov

Abstract

Black carbon (BC) particles exert a potentially large warming influence on the Earth system. Reductions in BC emissions have attracted attention as a possible means to moderate near-term temperature changes. For the first time, we evaluate regional climate responses, non-linearity, and short-term transient responses to BC emission perturbations in the Arctic, mid-latitudes, and globally based on a comprehensive set of emission-driven experiments using the Community Earth System Model (CESM). Surface temperature responses to BC emissions are complex, with surface warming over land from mid-latitude BC perturbations partially offset by ocean cooling. Climate responses do not scale linearity with emissions. While stronger BC emission perturbations have a higher burden efficiency, their temperature sensitivity is lower. BC impacts temperature much faster than greenhouse gas forcing, with transient temperature responses in the Arctic and mid-latitudes approaching a quasi-equilibrium state with a timescale of 2–3 years. We find large variability in BC-induced climate changes due to background model noise. As a result, removing present-day BC emissions results in discernible surface temperature changes for only limited regions of the globe. In order to better understand the climatic impacts of BC emissions, both the drivers of non-linear responses and response variability need to be assessed across climate models.

1. Introduction

Black carbon (BC) aerosol, emitted from incomplete combustion, may be the second strongest positive anthropogenic climate forcing following carbon dioxide, which drew attention for potential climate mitigation from reducing BC emissions (Jacobson, 2004; Shindell et al., 2012; Bond et al., 2013; Smith and Mizrahi, 2013). The relationship between forcing and surface temperature changes caused by BC is complex and forcing is not a reliable indicator of the climatic impact of BC emissions (Stjern et al., 2017). BC absorbs solar radiation within the atmospheric column thereby warming the atmosphere with an influence on surface temperature that depends on its vertical location. At high altitudes, BC cools the surface by absorbing solar radiation (i.e., blocking it from reaching the surface) (Ramanathan and Carmichael, 2008), while BC at low altitudes warms the surface through diabatic heating (Ban-Weiss et al., 2012). In addition, heating the atmosphere and cooling the surface can increase atmospheric stability and therefore affect cloud formation, lifetime, and dynamical processes (Koren et al., 2004; McFarquhar and Wang, 2006; Koch and Del Genio, 2010). Through transformation from hydrophobic aggregates to hydrophilic particles coated with water-soluble substances (*i.e.,* aging processes), BC can become cloud-nucleating particles (Oshima et al., 2009), alter cloud microphysical processes, and suppress precipitation (Boucher et al., 2013). BC-induced warming or cooling can increase or decrease surface evaporation, resulting in further changes in precipitation and cloud formation (McFarquhar and Wang, 2006; Andrews et al., 2010; Ming et al., 2010; Ban-Weiss et al., 2012;

Kvalevåg et al., 2013). BC can also decrease surface albedo through deposition on snow and ice, which is especially important to the climate at high latitudes and, particularly the Arctic (Flanner et al., 2007; Qian et al., 2014) as snow/ice-albedo effects are strong there. Taken together, these processes result in interactions between BC and the atmosphere that can ultimately alter the net impact of BC on climate, which have been termed rapid adjustments (Stjern et al., 2017).

Studies found that increases in BC emissions may contribute to the amplification of Arctic warming directly by absorbing solar radiation in the atmosphere and indirectly by reducing surface albedo through deposition on snow and ice (Flanner et al., 2007; Qian et al., 2014). Flanner (2013) highlighted the importance of BC vertical location in Arctic climate responses, with surface warming (cooling) due to BC in the lower (upper) troposphere. In addition, BC outside the Arctic can influence the Arctic climate through changing poleward heat transport. With BC snow/ice-albedo effect excluded, Shindell and Faluvegi (2009) modeled an Arctic surface warming (cooling) due to reducing (enhancing) mid-latitude BC atmospheric concentrations. Sand et al. (2013a) found that this was due to the increased northward heat transport into the Arctic. However, in another study where BC emissions were perturbed instead of concentrations, Sand et al. (2013b) reported a decrease in northward heat transport due to increases in mid-latitude BC emissions and suggested that the heating effect of BC transported to the Arctic dominated the Arctic heating in the mid-latitude perturbation simulation, leading to the opposite direction of atmospheric heat transport compared to the concentration-driven perturbations. They also found that

83 increases in both BC emission and BC concentration in the Arctic atmosphere may
84 weaken poleward heat transport due to increasing Arctic temperature driven by BC
85 heating in the atmosphere and on snow and ice surfaces. Therefore, understanding
86 the Arctic climate impact of regional BC emissions is important for the Arctic climate
87 mitigation (Sand et al., 2016).

88 In order to archive a statistically significant signal for Arctic surface temperature
89 responses to BC emissions, Sand et al. (2013b) scaled present-day BC emissions
90 within the Arctic by a factor of 150 and emissions from mid-latitudes by a factor of 9,
91 respectively, in the NorESM model with BC snow/ice-albedo effects included. They
92 found that emissions of BC within the Arctic have an Arctic surface temperature
93 response 5 times larger than those from mid-latitudes and attributed this to BC
94 snow/ice-albedo feedbacks. The impact of BC emission perturbations on
95 mid-latitudes were not examined in that study, which we do in this work to contrast
96 the impact of BC on the Arctic with mid-latitudes.

97 Much of the previous work on BC has used atmosphere-only models or
98 prescribed BC concentrations (Hansen et al., 2005; Ming et al., 2010; Ban-Weiss et
99 al., 2012; Sand et al., 2013a), which artificially reduces variability in model results.
100 Results qualitatively differ between prescribed BC-concentration and emission-driven
101 simulations with coupled models (Sand et al., 2013a,b, 2015). A previous study using
102 coupled models found that the BC response in three of these models showed high
103 variability and inconsistency in the net sign of the responses to present-day BC
104 emissions both between models and even between ensemble members from the

same model (Baker et al., 2015). Stjern et al. (2017) investigated climate responses to a tenfold increase in present-day anthropogenic BC concentrations or emissions using five concentration-driven and four emission-driven global climate models. They found that low-level cloud amounts increase, while higher-level clouds are diminished for all models, which is dominated by rapid adjustments. The negative rapid adjustments from changing clouds dampened positive instantaneous radiative forcing of BC at the TOA, leading to a relatively small global surface warming. However, this study did not consider response variability or non-linearity of responses. We note that the model used in our study contains a different aerosol treatment (see below) than the model used in Stjern et al. (2015).

To better understand the impacts of BC on climate, we present a comprehensive analysis using a set of coupled simulations that examine regional climate responses, non-linearity, and short-term transient climate responses to BC emission perturbations. We focus in particular on the Arctic and also variability to assess if climate responses to BC emission changes are likely to be discernable. Only combustion and process-based anthropogenic BC emissions are perturbed, given that the net global climate impact of open burning emissions has been assessed to be small due to their high organic carbon fraction. A summary of key results is provided below.

2. Methods

2.1 Model description

127 Here we use the fully coupled CESM (Community Earth System Model; Hurrell et
128 al., 2013) to simulate climate responses to BC emission perturbations. In
129 CAM5-MAM4 (Community Atmosphere Model version 5), the atmospheric
130 component of CESM, mass and number concentrations of aerosols are predicted
131 within four lognormal modes (i.e., Aitken, accumulation, coarse, and primary carbon
132 mode) of the modal aerosol module (MAM4; Liu et al., 2016). BC is emitted into the
133 primary-carbon mode and aged into the accumulation mode when coated with sulfate
134 or secondary organic aerosol. Particles in the accumulation mode, including BC and
135 other species, can serve as cloud condensation nuclei and have microphysical
136 effects on stratiform clouds and precipitation. The model physically treats
137 aerosol-cloud interactions using two-moment stratiform cloud microphysics, which
138 predicts number concentrations and mixing ratios of cloud water and ice (Morrison
139 and Gettelman, 2008; Gettelman et al., 2010). Activation of stratiform cloud droplets
140 is based on the scheme of Abdul-Razzak and Ghan (2000). In addition to the
141 standard treatments of aerosol-cloud interactions, we also include a set of
142 modifications that improves the simulation of aerosol wet scavenging and convective
143 transport (Wang et al., 2013). Although aerosols have no microphysical impact on
144 convective clouds, BC induced atmospheric heating can affect the ambient
145 temperature and convection. Convective precipitation can scavenge and remove
146 aerosols. Previous studies have extensively evaluated the CAM5 model simulations
147 of concentration, deposition, vertical profile and optical properties of BC (Wang et al.,
148 2013; Wang et al., 2015; Zhang et al., 2015a,b; Liu et al., 2016; Yang et al., 2017,

149 2018a,b)), as well as climate variables (Hurrell et al., 2013; Yang et al., 2016a,b).
150 The model can simulate well the BC aerosol and climate variables in most regions of
151 the globe, but was reported to underestimate BC concentrations over China (Yang et
152 al., 2018a) and the Arctic (Wang et al., 2013) (although this earlier study used a
153 different emissions dataset), implying a possible underestimate of climate responses
154 to BC emissions in this study.

155 In our model simulations, atmospheric radiative transfer is calculated twice with
156 BC included and excluded, respectively. The changes in direct radiative effect and
157 cloud radiative effect induced by BC perturbation are calculated as $\Delta(F_{clear} - F_{clear,clean})$
158 and $\Delta(F_{clean} - F_{clear,clean})$, respectively, where F_{clear} is the TOA flux calculated
159 neglecting scattering and absorption by clouds, F_{clean} is the TOA flux calculated
160 neglecting scattering and absorption by BC, $F_{clear,clean}$ is the TOA flux calculated
161 neglecting scattering and absorption by both clouds and BC, and Δ refers to the
162 differences between the control and one of the emission perturbed simulations (Ghan,
163 2013). Note that these quantities include the impact of slow responses and feedbacks
164 (e.g., changes in sea surface temperature and sea ice and feedbacks with clouds) so
165 are not strictly comparable to the conventional definition of radiative forcing (Boucher
166 et al., 2013). The BC snow/ice-albedo effect on top of land and sea ice is included in
167 the model (Flanner et al., 2007; Yang et al., 2017, 2018c).

168 **2.2 Experimental configuration and emissions**

169 The following simulations are performed in this study. All insolation, greenhouse
170 gas concentrations and aerosol and precursor emissions, except BC, are fixed at
171 year 1850 levels, which include open burning emissions (van Marle et al., 2017).
172 The MID7X and ARC150X simulations use large emission perturbations to result
173 in signals large enough for detailed analysis. These regions are also particularly
174 important for BC impacts on the Arctic. The multipliers were selected following Sand
175 et al. (2013b) with the expectation that these would result in similar radiative
176 perturbations. This also allows a direct comparison to these previous results (Sand et
177 al., 2013b; and also Baker et al., 2015), which are also BC-emission simulations
178 using a coupled model with snow/ice-albedo feedbacks. The PD simulation then
179 allows us to evaluate the impact of present-day anthropogenic emissions. In brief, the
180 simulations conducted are:
181 1. PD: control simulation for BC in present-day conditions. BC emissions are
182 fixed at year 2010 (average of 2008–2012).
183 2. ARC150X: perturbed simulation to quantify the climate responses to Arctic BC
184 emissions. Same as PD except that year 2010 level anthropogenic BC
185 emissions over the Arctic (60–90°N) are scaled by a factor of 150.
186 3. MID7X: perturbed simulation to quantify the climate responses to mid-latitude
187 BC emissions. Same as PD except that year 2010 level anthropogenic BC
188 emissions over the mid-latitudes (28–60°N) are scaled by a factor of 7.

4. ARC75X: perturbed simulation to quantify non-linearity of climate responses to Arctic BC emissions. Same as ARC150X except that Arctic BC emissions are scaled by a factor of 75.
5. MID3.5X: perturbed simulation to quantify non-linearity of climate responses to mid-latitude BC emissions. Same as MID7X except that mid-latitude BC emissions are scaled by a factor of 3.5.
6. MID14X: perturbed simulation to quantify non-linearity of climate responses to mid-latitudes BC emissions. Same as MID7X except that mid-latitude BC emissions are scaled by a factor of 14.
7. PI: sensitivity simulation for BC in preindustrial conditions to compare results with Baker et al. (2015). BC emissions are at year 1850 levels.

Both mass and number of BC emissions are perturbed proportionally. Each simulation has one ensemble member for 100 years which are branched from year 81 of the PI simulation after 80 years spin-up, with the last 80 years used for most analysis. Another four short-term ensemble members for 30 years are conducted under both ARC150X and MID7X to examine the short-term transient climate response to BC emissions. These are branched from years 96, 112, 120, and 140 of PI simulation.

The CEDS (Community Emissions Data System) anthropogenic emissions (Hoesly et al., 2018) (version 2017-05-18) that were developed for the CMIP6 (Coupled Model Intercomparison Project Phase 6) model experiments are used in our simulations. Note that this emission dataset includes monthly BC emission

211 seasonality, which has been shown to be important for simulating BC in the Arctic
212 (Stohl et al., 2013). Figure S1 shows spatial distribution of annual anthropogenic BC
213 emissions for year 2010 (average of 2008–2012) and the regions for BC emission
214 perturbation. Over 60–90°N, anthropogenic BC emissions are mostly over the lower
215 latitude of the Arctic (60–70°N). Over the mid-latitudes, high BC emissions are mainly
216 located over eastern China. The annual total anthropogenic BC emission from the
217 Arctic in year 2010 is 0.08 Tg C yr^{-1}, with 70% contributed by energy sector. Scaled
218 by a factor of 150, ARC150X has 12.63 Tg C yr^{-1} more BC emissions than the PD in
219 the Arctic. About 3.46 Tg C yr^{-1} of BC is emitted from the mid-latitudes, with the
220 largest contribution from the residential sector (36%). With a scaling factor of 7,
221 MID7X includes an additional 20.74 Tg C yr^{-1} of BC emission from mid-latitudes, as
222 compared to PD. Global annual anthropogenic BC for PD is 7.72 Tg C yr^{-1}, much
223 higher than 0.92 Tg C yr^{-1} for PI.
224
225 **3. Regional climate responses to increases in Arctic and mid-latitude BC**
226 **emissions**
227 We first examine results from simulations with large perturbations of Arctic and
228 mid-latitude BC emissions (ARC150X and MID7X). Our initial simulations focused on
229 these regions due to the potentially high sensitivity of the Arctic to BC emissions.
230 Figure 1 presents the increases in annual, zonal-mean BC concentrations from
231 ARC150X and MID7X simulations, as compared to PD. Both Arctic and mid-latitude
232 BC emissions lead to BC concentration increases in the entire Northern Hemisphere,

with Arctic emissions mainly impacting low altitudes within the Arctic. In ARC150X, due to extremely low temperatures at the surface and therefore temperature inversions and a transport barrier (so called Arctic front), BC concentration increases are mainly located over low altitudes within the Arctic. In MID7X, increased mid-latitude emissions produce large increases in BC concentrations between 30°–45°N. BC emitted over the mid-latitudes, which is lifted above the boundary layer and transported at higher altitudes into the Arctic, leading to increased concentrations of BC in the Arctic atmosphere. This spatial pattern is similar to that in Sand et al. (2013b).

To explore the importance of emissions from these source regions to BC column burdens, Table 1 summarizes BC burden efficiency, which is defined as the changes in regional mean column burden of BC produced by per unit emission change, calculated by differences between the perturbed and PD simulation. Over the Arctic, increases in Arctic local BC emissions lead to an Arctic column burden efficiency of 0.425 ±0.024 mg m^{-2} (Tg yr^{-1})$^{-1}$. The burden efficiency of mid-latitude emissions over the mid-latitudes is 0.191 ±0.004 mg m^{-2} (Tg yr^{-1})$^{-1}$, less than half of the efficiency of Arctic emission on Arctic burden due to lower precipitation and frequent temperature inversion in the Arctic compared to mid-latitudes. While the relative impact of mid-latitude emissions on the Arctic burden efficiency (0.106 ±0.004 mg m^{-2} (Tg yr^{-1})$^{-1}$) is smaller than either of the above efficiencies, the 28 times larger present-day total emissions from mid-latitudes (3.70 Tg yr^{-1}) than the Arctic (0.13 Tg yr^{-1}) dominate column burden contributions.

255 Table 1 also summarizes the changes in BC direct radiative effect, cloud radiative
256 effect, and snow/ice-albedo forcing induced by these large BC perturbations. Note
257 that these values include feedback effects from the coupled system, so are not
258 comparable to conventionally defined radiative forcing values. The albedo change
259 due to BC deposition on snow and ice is responsible for a significant increase in
260 Arctic surface forcing in both perturbations, with far smaller changes per unit emission
261 in mid-latitudes. Positive changes in direct radiative effect are offset by negative
262 changes in cloud radiative effect from increases in low cloud in the Arctic and
263 decreases in mid-level and high cloud over the mid-latitudes, similar to previous
264 results with a tenfold increase in present-day anthropogenic BC emissions (Stjern et
265 al., 2017).
266 Forcing efficiencies for direct radiative effect, cloud radiative effect and
267 snow/ice-albedo forcing (i.e., forcings produced by per unit emission change) are also
268 summarized in Table 1. Over the Arctic, local emissions from the Arctic have 2–4
269 times higher forcing efficiencies than emissions from the mid-latitudes, suggesting
270 higher impacts of a unit Arctic BC emission change to Arctic energy balance. Over the
271 mid-latitudes, although forcing efficiencies for direct radiative and cloud radiative
272 effects for Arctic emissions are 2–3 times lower than mid-latitude emissions, the
273 snow/ice-albedo forcing efficiencies are similar between Arctic and mid-latitude
274 emissions.
275 The annual mean surface air temperature response in ARC150X shows a
276 significant warming over both the Arctic and mid-latitudes (Figure 2). MID7X shows

277 temperature increases over the Arctic and most of the mid-latitude land regions, while
278 surface temperature decreases over some oceanic and coastal areas. The presence
279 of areas with both surface warming and cooling decreases the net average
280 temperature change over mid-latitudes. The seasonal mean surface air temperature
281 responses present similar spatial patterns (Figure S2), but slightly different
282 magnitudes (Figure S3). Over the Arctic, the warming due to Arctic BC emissions is
283 weakest in boreal summer. This is because the smaller summer sea ice and snow
284 fraction in the Arctic weakens BC snow/ice-albedo forcing. However, in the
285 mid-latitudes, warming is strongest in boreal summer for both Arctic and mid-latitude
286 BC emissions, because of stronger summer solar insolation and, therefore, stronger
287 BC heating in the atmosphere.

288 Due to the increased atmospheric absorption from BC, northward heat transport
289 for both perturbations decreases (Figure 3), consistent in sign with the results of Sand
290 et al. (2013b). The increases in temperature but decreases in net northward heat
291 transport indicate that the heating induced by changes in BC direct radiative effect
292 and BC snow/ice-albedo forcing dominate the overall BC-induced changes in energy
293 balance over the Arctic and mid-latitudes.

294 Arctic emissions are more efficient at impacting Arctic surface air temperatures
295 with an Arctic temperature sensitivity to Arctic emissions (0.169 ±0.052 K (Tg yr^{-1})$^{-1}$)
296 seven times as large as the Arctic temperature sensitivity to mid-latitude emissions
297 (0.023 ±0.038 K (Tg yr^{-1})$^{-1}$). Mid-latitude emissions, however, are likely to have a
298 larger present-day impact overall due to their 35 times larger preindustrial to

299 present-day emission increase (2.874 Tg yr^{-1}) than Arctic emissions (0.082 Tg yr^{-1}).
300 Note that, the Arctic temperature sensitivities are about 30% and 50% smaller than
301 those found in the coupled NorESM model experiments of Sand et al. (2013b) for
302 Arctic and mid-latitude emission perturbation simulations, respectively, probably due
303 to different model parameterizations and/or different vertical profile of BC driving the
304 net effect of BC impact on Arctic surface temperature (Flanner, 2013).

305 The vertical distribution of annual, zonal mean temperature responses (Figure 4)
306 shows that the ARC150X leads to a strong warming from the surface to 400 hPa over
307 the Arctic and between 40°–60°N. In MID7X, although the zonal mean surface
308 temperature response is relatively weak compared to ARC150X, a significant
309 warming is found in mid-latitudes between 500 and 200 hPa. BC transported from
310 mid-latitudes into the Arctic at high altitudes also results in Arctic temperature
311 increases aloft, between 400 and 300 hPa.

312 These changes in temperature pattern can change the stability of the atmosphere
313 and impact atmospheric circulation, as shown in Figure 5. Increases in BC emissions
314 over both the Arctic and mid-latitudes exert anomalous upward motions in the Arctic
315 and downward motions over the mid-latitudes, but for different reasons. In ARC150X,
316 stronger warming at the Arctic surface, compared to high altitudes, likely due to the
317 BC snow/ice-albedo effect, produces anomalous upward motions in the Arctic and
318 compensating downward motions between 50°–60°N. In MID7X, the stronger BC
319 warming at higher altitudes in mid-latitudes increases atmospheric stability and leads
320 to strong anomalous downward motions between 40°–60°N and compensating

upward motions over the Arctic and 10°–30°N (Johnson et al., 2004). Increasing surface temperature and anomalous upward motion over the Arctic can weaken the Arctic front, and the anomalous downward motion over the mid-latitudes favors air stagnation.

Because of the anomalous downward motions over mid-latitudes in both ARC150X and MID7X, high and/or mid-level cloud fraction decrease over mid-latitudes (Figure 6). Due to slow feedbacks from increases in surface temperature in the Arctic (Figure 2) and decreases in snow and sea ice, low cloud fraction increases in the Arctic for both ARC150X and MID7X. The increases in low cloud over mid-latitude oceans, which cause the cooling noted above, are due to rapid adjustments as free-tropospheric BC heating reduces mixing with dry air above the BC layer and increases the amount of marine stratocumulus (Johnson et al., 2004; Sand et al., 2013a; Stjern et al., 2017).

Figure 7 shows changes in the total precipitation rate for the perturbed simulations. Increases in Arctic and mid-latitude BC emissions lead to significant decreases in precipitation over 60°N and 30–50°N, respectively, in correspondence with anomalous downward motions (Figure 5) and decreases in mid-level and high clouds (Figure 6) over these regions. Averaged over the Arctic and mid-latitudes, changes in precipitation are weak, compared to uncertainties, except for the mid-latitude precipitation response to BC emitted from mid-latitudes. The mid-latitude precipitation sensitivity is –7.67 (±3.34) μm day^{-1} (Tg yr^{-1})$^{-1}$ for MID7X. Another feature of the precipitation response is related to a northward shift in the ITCZ

(Intertropical Convergence Zone) in MID7X, which is consistent with the hemispherically asymmetric warming pattern driven by increases in mid-latitude BC emissions (Hwang et al., 2013; Baker et al., 2015).

Both ARC150X and MID7X show significant decreases by 13% and 3%, respectively, in fractional area covered by sea ice over the Arctic, as compared to PD (Figure S4). The snow depth over land also decreases, especially over Greenland. The water equivalent snow depth averaged over Arctic land decreases by 5.0 cm (27% relative to PD) and 0.8 cm (4%), respectively, for ARC150X and MID7X.

4. Non-linearity of climate responses.

We also evaluated the linearity of these responses by testing different emission perturbation sizes. Figure 8 shows burden efficiencies, temperature and precipitation sensitivities from simulations with Arctic BC emissions scaled by 75 and 150, respectively, and mid-latitude BC emissions scaled by 3.5, 7 and 14, respectively, with values summarized in Table 2. Stronger emission perturbations have a higher burden efficiency. Over the Arctic, this is caused by anomalous Arctic upward motions that weaken the Arctic front, lifting BC higher and leading to a longer BC lifetime together with easier transport into the Arctic (Figure S5). Over mid-latitudes, anomalous mid-latitude downward motions favor stagnation, which in turn accumulates more BC in the atmosphere, together with decrease in precipitation (and wet removal rate), contributing to increases in burden efficiency. All differences in

364 burden efficiencies between simulations with different emission perturbation sizes are
365 statistically significant with 95% confidence.
366 Despite this higher burden efficiency, the efficiency (per unit emission) of the
367 direct radiative effect decreases slightly. This is because strong BC perturbations
368 lead to more BC suspended in the atmosphere. More BC increases the attenuation of
369 the transmitted radiation, leading to a decrease in efficiency of BC light absorption in
370 the lower atmosphere and leading to a lower efficiency of direct radiative effect for a
371 stronger BC emissions perturbation.
372 The temperature sensitivity is lower, with 95% significance, for stronger
373 emission perturbations for both mid-latitude and Arctic BC between ARC75X and
374 ARC150X, as well between MID7X and MID14X (Table 2). The BC snow/ice-albedo
375 effect is found to be the most important factor in influencing Arctic temperature (Sand
376 et al., 2013b). Larger temperature increases from stronger BC emission perturbations
377 speed up sea ice and snow melt, leading to a weaker annual mean snow/ice-albedo
378 effect per unit BC emission for both Arctic and mid-latitudes. Therefore, the BC
379 snow/ice-albedo effect is more efficient for weaker emission perturbations, i.e., 0.151
380 (±0.011) vs. 0.099 (±0.006) (W m^{-2} (Tg yr^{-1})$^{-1}$) for ARC75X and ARC150X and 0.026
381 (±0.002) vs. 0.020 (±0.002) (W m^{-2} (Tg yr^{-1})$^{-1}$) for MID7X and MID14X of Arctic BC
382 snow/ice-albedo forcing efficiencies. All snow/ice-albedo forcing efficiency
383 differences are statistically significant. Together with lower efficiency of the direct
384 radiative effect, these explain the lower temperature sensitivity for stronger emission
385 perturbation. The non-linearity in snow-ice feedback relative to emissions size

386 appears to be the primary driver of surface temperature response non-linearity in
387 these results.
388 Additional evidence for BC non-linearity can be found in the literature. Sand et al.
389 (2015) simulated climate responses to BC in NorESM with present-day emissions
390 multiplied by 25 and reported that the changes in TOA net shortwave flux was 7.5
391 (±0.3) W m^{-2} relative to preindustrial conditions and the temperature response was
392 1.2 (±0.1) K. If we assume a linear emission-response relationship, present-day BC
393 would cause an inferred shortwave flux and surface temperature change of 0.312
394 (±0.013) W m^{-2} and 0.050 (±0.004) K in Sand et al. (2015), much lower than the 0.552
395 W m^{-2} and 0.141 K found in Baker et al. (2015) for a present-day BC emission
396 perturbation with essentially the same model. Note that the change in shortwave flux
397 is not proportional to the surface temperate change, further emphasizing that forcing
398 is not a good predictor of surface temperature change for BC. This comparison is
399 consistent with our finding that temperature sensitivity is lower for stronger BC
400 emission perturbations. We note, however, that emission datasets with different
401 spatial distributions and seasonality were used in those two experiments (because of
402 this the difference in global emissions between the two experiments is about 17, not
403 25 times). While this might impact the magnitude of model responses, it is unlikely to
404 change the overall conclusion of a substantially different temperature response to
405 current-day emissions as compared to a 17–25 times larger BC perturbation.
406 The mid-latitude shows significantly stronger precipitation sensitivity for a
407 stronger perturbation, comparing MID7X and MID14X, which is consistent with the

higher burden efficiency. This is in the opposite direction to the surface temperature sensitivity. Variability in MID3.5X is larger than the mean value for both temperature and precipitation sensitivity, which highlights the challenge of testing differences for smaller BC perturbation magnitudes. Note that the impact of BC on clouds and precipitation is uncertain, especially in the Arctic, due to the limited treatment of Arctic clouds in climate models (McFarquhar et al., 2011). These results suggest that in order to examine the climate responses to BC emissions in short-term climate model simulations, a large emission perturbation is needed to get a clear signal, but non-linearity of the responses also needs to be evaluated.

5. Short-term transient climate responses

To assess the short-term transient climate responses to BC emissions, Figure 9 shows surface temperature responses to BC emissions from ARC150X and MID7X for the first 30 years averaged over five short ensemble members. We also show a numerical fit to the short-term transient response using a Hamiltonian Monte Carlo technique (Betancourt, 2017). We fit to the following form:

$$T_{ave}\,(1 - e^{-t/\tau}),$$

where we have constrained the fit to converge to the long-term average temperature response (T_{ave}) by our finding that there is no detectable long-term trend after the initial transient period over a 100-year time horizon.

Over both the Arctic and mid-latitudes, transient temperature responses quickly approach a quasi-equilibrium state. Transient timescales (τ) for the ARC150X

perturbation were estimated to be 2.7 (2.0, 3.4) years, while the mid-latitude timescales for the ARC150X and MID7X perturbations were 1.8 (1.1, 2.2) and 2.9 (1.2, 4.2) years respectively (brackets provide 10-90% fitting intervals). The Arctic response to MID7X was too noisy to produce a fit. These timescales are shorter than those in a global BC perturbation experiment (Sand et al., 2015), which is expected as ocean thermal inertia would play a larger role globally as compared to the Northern Hemisphere or Arctic. The BC response timescales here are also shorter than those seen from CO_2 concentration steps in GCMs (Geoffroy et al., 2013). There is also no long-term temperature increase, at least over a 100-year time horizon, after the initial transient period. A linear fit over years 10-100 for the perturbation responses results in no statistically significant linear trends for any of the four perturbations (see SI code).

Note that the average of even five ensemble members shows oscillatory behavior due to the imposition of a step BC emission perturbation. This oscillatory behavior degrades our ability to quantify the perturbation response timescale. In future work, a linearly phased-in perturbation might result in a cleaner signal for determining the initial response time-scale.

6. Climate responses to present-day anthropogenic BC emissions

Baker et al. (2015) showed that the climate responses to BC emissions had very large uncertainties based on results from four global models. Here, we also quantified the impact of present-day anthropogenic BC emissions (Figure 10) by comparing a

present-day (PD) and pre-industrial (PI) simulation conducted with the CESM-CAM5-MAM4 model used in this work. PD emissions produce statistically significant surface air temperature changes over only limited regions in the Northern Hemisphere. Decreased temperatures are found over eastern China, South Asia, North Atlantic Ocean, and North American Arctic, partly due to cloud changes driven by BC rapid adjustments. Increased temperatures are found over the Tibetan Plateau, Greenland and high-latitude land regions likely because of the BC snow/ice-albedo effect (Figure S6).

The spatial pattern is similar to that from the ECHAM6-HAM2 in Baker et al. (2015). Although CESM-CAM5-MAM4 also includes the BC snow/ice-albedo effect, we do not see the strong warming produced in NorESM under present-day BC emissions. In Baker et al. (2015), NorESM had a global net TOA shortwave forcing efficiency of 0.076 W m^{-2} (Tg yr^{-1})$^{-1}$, nominally higher than 0.043 ±0.073 W m^{-2} (Tg yr^{-1})$^{-1}$ calculated in this study with CESM-CAM5-MAM4, although the difference is well within one standard deviation. Longer model runs would be needed to determine if the BC snow/ice-albedo effect is significantly different in CESM and NorESM. In addition, there may be a small contribution from a shorter BC lifetime (7.22 days in CESM-CAM5-MAM4 Vs. 7.82 days in NorESM) that might also help explain the weaker warming in CESM-CAM5-MAM4 as compared to NorESM.

We find that variability is substantial in our experiments. Although statistically significant surface temperature changes are found regionally, as mentioned above, large-scale global surface temperature change from current-day BC emissions is

474 statistically indistinguishable from zero (0.006 ±0.238 K globally and 0.020 ±0.346 K
475 for land only). The global temperature response is within the range of –0.085 to 0.152
476 K from the four models in Baker et al. (2015). Even in the large MID7X perturbation,
477 variability is still fairly large relative to the signal (0.45 ±0.27 K for mid-latitude
478 temperate change) and would overwhelm any large-scale signal for more realistic
479 perturbation sizes. Similarly, while the mid-latitude precipitation response to
480 mid-latitude BC emissions is strong for a MID7X perturbation, this would be difficult to
481 detect for a present-day perturbation.
482
483 **7. Conclusions and discussions**
484 BC has been estimated to potentially have one of the largest positive (warming)
485 anthropogenic forcing influences. As a result, there has been substantial scientific
486 and policy attention focused on the potential for BC to moderate climate change in the
487 near-term. In this study, for the first time, we conduct a comprehensive set of
488 emission-driven experiments using a leading coupled climate model (CESM). With a
489 comprehensive set of experiments, we examined regional climate responses,
490 non-linearity, and short-term transient responses to BC emission perturbations in the
491 Arctic, mid-latitudes, and globally.
492 With increases in mid-latitude BC emissions, surface air temperature increases
493 over land, while it decreases over oceanic and coastal areas. Increases in Arctic BC
494 emissions lead to warming over both the Arctic and mid-latitudes. Increases in Arctic
495 and mid-latitude BC emissions also decrease precipitation over 60°N and 30–50°N,

496 respectively. Arctic emissions are more efficient in influencing Arctic surface air
497 temperatures compared to mid-latitude emissions, with an Arctic temperature
498 sensitivity to Arctic emissions seven times as large as that to mid-latitude emissions.
499 We find that climate responses do not scale linearity with emissions. While
500 stronger BC emission perturbations have a higher burden efficiency, efficiencies of
501 snow/ice-albedo forcing and direct radiative effect are lower, leading to a lower
502 temperature sensitivity for stronger BC emission perturbations.
503 BC also impacts temperature much faster than greenhouse gas forcing, with
504 transient temperature responses in the Arctic and mid-latitudes approaching a
505 quasi-equilibrium state with a timescale of 2–3 years. While it has previously been
506 found that, globally, aerosols have a faster impact on temperature as compared to
507 greenhouse gases (Shindell., 2014), termed a “geometric effect” (Meinshausen et al.,
508 2011), we find here that BC perturbations have a very short response time,
509 particularly for Arctic and mid-latitude perturbations. This means that previous studies
510 which have implicitly assumed that the temperature response timescales of BC and
511 GHGs are the same (Boucher and Reddy 2008, Stohl et al., 2015) have likely
512 underestimated the short-term impact of BC emission changes.
513 We find large variability in BC-induced climate changes. Baker et al. (2015)
514 provided error bars of global temperature response for different models in their Figure
515 4a. We note, however, that the error bars in Baker et al. are underestimated because
516 of their assumption of independence of all annual data points (note their use of
517 1σ/sqrt(N) in their error bars for Figure 4). Climate model surface temperatures are

518 strongly correlated over short time scales, which means that instead of the number of
519 data points, a more appropriate measure is the effective number of independent data
520 points (N_{eff}). The 100-year model runs examined here do not provide enough data for
521 this calculation. (Note that we were able to estimate N_{eff} for the 300-year CESM
522 control run from CMIP5, which indicates that runs around 3 times as long as those
523 presented here may be necessary). We, therefore, present standard deviation as a
524 metric of variance.

525 The standard deviation (SD) of global mean surface temperature in PI, PD, and in
526 all of our perturbed simulations is around 0.17–0.19 K, indicating that the dominant
527 source of temperature variability is probably due to internal climate variability or
528 model noise. The SD for temperature responses in perturbed simulations relative to
529 PD are in ranges of 0.24–0.26, roughly 1.4 times the control run temperature
530 variability. This is in the expectation from subtracting two independent Gaussian
531 noise distributions. While there could be an additional contribution to variability from
532 BC-climate interactions, this appears to be small in this case given the relatively small
533 surface temperature response to BC. We also observe large variability in cloud
534 radiative effects, which we note may be impacted by interactions with BC.

535 While we have demonstrated non-linear responses at high emission levels, this
536 non-linearity is not sufficient to produce statistically significant global temperature
537 changes from present-day BC emissions in this model. Such non-linearities mean
538 that the implications of large BC emission perturbation experiments, such as recent
539 tenfold BC experiments (Stjern et al., 2017) for present-day conditions are unclear.

While snow/ice-albedo feedbacks appear to dominate the non-linear relationship in these results, this may not be the case in other models.

Our results point to the importance of better quantifying the variability in BC responses in the Earth system. We note that in the one model with a consistent PD-PI signal in a set of recent PD-PI BC experiments (NorESM1-M), the size of that signal is still smaller than the variability found here, based on similar SD in Arctic temperature change for the ARC150X simulations in the two models (compare Figure S3 here with Figure 9 in Sand et al. (2013b)). If the global variability of BC response in NorESM is also similar to that in CESM, then the global average temperature change from NorESM (0.141 K) (Baker et al., 2015) is also much smaller than the SD in CESM of 0.238 K. However, we do note that there was a fair degree of consistency in temperature change signal in NorESM between two ensemble members (0.129 K and 0.152 K). This may mean that variability in the global BC response in the NorESM model could be smaller than seen in our results due to the stronger NorESM BC temperature response. Longer simulations would likely be required to assess this. While, compared to temperature or precipitation, aerosol burdens, BC direct radiative effects and snow/ice-albedo forcings have much larger signal to noise ratios, i.e. ratio of mean response to standard deviation (Table 1), and can be useful as diagnostics, BC forcing does not provide a reliable indicator of surface temperature changes across models.

These results indicate that even substantial BC emissions reductions from current levels may lead to detectable surface temperature changes for only limited

562 regions of the globe. Our results have significant implications for near-term climate
563 mitigation associated with BC as well as global and regional climate attribution. We
564 note that regional climate sensitivities (RCS), used as an approximate approach to
565 represent the impact of BC (Collins et al., 2013; Sand et al., 2016), are generally
566 evaluated using model simulations with prescribed forcing or burdens (Shindell and
567 Faluvegi, 2009), which artificially reduce response variability and imply a certainty in
568 BC responses that may not exist in reality. Variability within any given model run,
569 which has generally not been reported in current literature, is large relative to BC
570 responses. It is, therefore, not clear if current BC emission levels result in statistically
571 significant large-scale climatic changes. We suggest that impacts of BC on climate
572 should be expressed directly in terms of impacts per unit emissions (e.g. Table 1),
573 and not only relative to forcing given the complex relationship between BC climatic
574 impacts and top of the atmosphere forcing. In addition, BC impacts should be
575 re-evaluated using coupled models, and provided with measures of response
576 variability, such as standard deviation. In order to better assess the potential impact
577 of changes in BC emissions it is critical to quantify the non-linearity of BC response
578 efficiencies with respect to emission perturbation size in other models, as well as the
579 causes of those non-linearities.
580

Data availability.

All the emissions data sets used in this study can be obtained from https://esgf-node.llnl.gov/search/input4mips/ (Hoesly et al., 2018; van Marle et al., 2017). The CESM model is publicly available at http://www.cesm.ucar.edu/models/cesm1.2/ (Hurrell et al., 2013). Our model results can be made available through the National Energy Research Scientific Computing Center (NERSC) servers upon request.

Competing interests.

The authors declare that they have no conflict of interest.

Author contribution.

YY, SJS and HW designed the research; YY performed the model simulations; YY, and SJS analyzed the data. All the authors discussed the results and wrote the paper.

Acknowledgments.

This research is based on work that was supported by the U.S. Environmental Protection Agency, and the U.S. Department of Energy (DOE), Office of Science, Biological and Environmental Research as part of the Regional and Global Climate Modeling program. The Pacific Northwest National Laboratory is operated for DOE by Battelle Memorial Institute under contract DE-AC05-76RLO1830. The National Energy Research Scientific Computing Center (NERSC) provided computational support.

References

Abdul-Razzak, H. and Ghan, S. J.: A parameterization of aerosol activation 2. Multiple aerosol types, J. Geophys. Res., 105, 6837–6844, doi:10.1029/1999JD901161, 2000.

Andrews, T., Forster, P. M., Boucher, O., Bellouin, N., and Jones, A.: Precipitation, radiative forcing and global temperature change, Geophys. Res. Lett., 37, L14701, doi:10.1029/2010GL043991, 2010.

Baker, L. H., Collins, W. J., Olivié, D. J. L., Cherian, R., Hodnebrog, Ø., Myhre, G., and Quaas, J.: Climate responses to anthropogenic emissions of short-lived climate pollutants, Atmos. Chem. Phys., 15, 8201-8216, doi:10.5194/acp-15-8201-2015, 2015.

Ban-Weiss, G. A., Cao, L., Bala, G., and Caldeira, K.: Dependence of climate forcing and response on the altitude of black carbon aerosols, Clim. Dyn., 38, 897–911, doi:10.1007/s00382-011-1052-y, 2012.

Betancourt, M.: A conceptual introduction to Hamiltonian Monte Carlo, arXiv preprint, arXiv:1701.02434, 2017.

Bond, T. C., Doherty, S. J., Fahey, D. W., Forster, P. M., Berntsen, T., DeAngelo,B. J., Flanner, M. G., Ghan, S., Kärcher, B., Koch, D., Kinne, S., Kondo, Y., Quinn, P. K., Sarofim, M. C., Schultz, M. G., Schulz, M., Venkataraman, C., Zhang, H., Zhang, S., Bellouin, N., Guttikunda, S. K., Hopke, P. K., Jacobson, M. Z., Kaiser, J. W., Klimont, Z., Lohmann, U., Schwarz, J. P., Shindell, D., Storelvmo, T., Warren, S. G., and Zender, C. S.: Bounding the role of black carbon in the climate system: A scientific assessment, J. Geophys. Res., 118, 5380–5552, doi:10.1002/jgrd.50171, 2013.

Boucher, O., Randall, D., Artaxo, P., Bretherton, C., Feingold, G., Forster, P., Kerminen, V.-M., Kondo, Y., Liao, H., Lohmann, U., Rasch, P., Satheesh, S. K., Sherwood, S., Stevens, B., and Zhang, X. Y.: Clouds and Aerosols, in: Climate Change 2013: The Physical Science Basis, Contribution of Working Group I to the Fifth Assessment Report of the Intergovernmental Panel on Climate Change, edited by: Stocker, T. F., Qin, D., Plattner, G.-K., Tignor, M., Allen, S. K., Boschung, J., Nauels, A., Xia, Y., Bex, V., and Midgley, P. M., Cambridge University Press, Cambridge, United Kingdom and New York, NY, USA, 571–658, doi:10.1017/CBO9781107415324.016, 2013.

Boucher, O. and Reddy, M. S.: Climate trade-off between black carbon and carbon dioxide emissions, Energ. Policy, 36, 193–200, doi:10.1016/j.enpol.2007.08.039, 2008.

Collins, W. J., Fry, M. M., Yu, H., Fuglestvedt, J. S., Shindell, D. T., and West, J. J.: Global and regional temperature-change potentials for near-term climate forcers, Atmos. Chem. Phys., 13, 2471-2485, https://doi.org/10.5194/acp-13-2471-2013, 2013.

Flanner, M. G.: Arctic climate sensitivity to local black carbon, J. Geophys. Res. Atmos., 118, 1840–1851, doi:10.1002/jgrd.50176, 2013.

Flanner, M. G., Zender, C. S., Randerson, J. T., and Rasch, P. J.: Present day climate forcing and response from black carbon in snow, J. Geophys. Res., 112, D11202, doi:10.1029/2006JD008003, 2007.

Geoffroy, O., Saint-Martin, D., Bellon, G., Voldoire, A., Olivié, D. J., and Tytéca, S.: Transient climate response in a two-layer energy-balance model. Part II: Representation of the efficacy of deep-ocean heat uptake and validation for CMIP5 AOGCMs, J. Climate, 26, 1859–1876, doi:10.1175/JCLI-D-12-00196.1, 2013.

Gettelman, A., Liu, X., Ghan, S. J., Morrison, H., Park, S., Conley, A. J., Klein, S. A., Boyle, J., Mitchell, D. L., and Li, J. L. F.: Global simulations of ice nucleation and ice supersaturation with an improved cloud scheme in the Community Atmosphere Model, J. Geophys. Res., 115, D18216, doi:10.1029/2009jd013797, 2010.

Ghan, S. J.: Technical Note: Estimating aerosol effects on cloud radiative forcing, Atmos. Chem. Phys., 13, 9971–9974, doi:10.5194/acp-13-9971-2013, 2013.

Hansen, J., Sato, M., Ruedy, R., Nazarenko, L., Lacis, A., Schmidt, G. A., Russell, G., Aleinov, I., Bauer, M., Bauer, S., Bell, N., Cairns, B., Canuto, V., Chandler, M., Cheng, Y., Del Genio, A., Faluvegi, G., Fleming, E., Friend, A., Hall, T., Jackman, C., Kel- ley, M., Kiang, N., Koch, D., Lean, J., Lerner, J., Lo, K., Menon, S., Miller, R., Minnis, P., Novakov, T., Oinas, V., Perlwitz, Ja., Perlwitz, Ju., Rind, D., Romanou, A., Shindell, D., Stone, P., Sun, S., Tausnev, N., Thresher, D., Wielicki, B., Wong, T., Yao, M., and Zhang, S.: Efficacy of climate forcings, J. Geophys. Res., 110, D18104, doi:10.1029/2005JD005776, 2005.

Hoesly, R. M., Smith, S. J., Feng, L., Klimont, Z., Janssens-Maenhout, G., Pitkanen, T., Seibert, J. J., Vu, L., Andres, R. J., Bolt, R. M., Bond, T. C., Dawidowski, L., Kholod, N., Kurokawa, J.-I., Li, M., Liu, L., Lu, Z., Moura, M. C. P., O'Rourke, P. R., and Zhang, Q.: Historical (1750–2014) anthropogenic emissions of reactive gases and aerosols from the Community Emissions Data System (CEDS), Geosci. Model Dev., 11, 369–408, doi:10.5194/gmd-11-369-2018, 2018.

690 Hurrell, J. W., Holland, M. M., Gent, P. R., Ghan, S., Kay, J. E., Kushner, P. J.,
691 Lamarque, J. F., Large, W. G., Lawrence, D., Lindsay, K., Lipscomb, W. H., Long,
692 M. C., Mahowald, N., Marsh, D. R., Neale, R. B., Rasch, P., Vavrus, S.,
693 Vertenstein, M., Bader, D., Collins, W. D., Hack, J. J., Kiehl, J., and Marshall, S.:
694 The Community Earth System Model A Framework for Collaborative Research, B.
695 Am. Meteorol. Soc., 94, 1339–1360, doi:10.1175/BAMS-D-12-00121.1, 2013.
696
697 Hwang, Y.-T., Frierson, D. M. W., and Kang, S. M.: Anthropogenic sulfate aerosol
698 and the southward shift of tropical precipitation in the late 20th century, Geophys.
699 Res. Lett., 40, 2845–2850, doi:10.1002/grl.50502, 2013.
700
701 Jacobson, M. Z.: Climate response of fossil fuel and biofuel soot, accounting for
702 soot's feedback to snow and sea ice albedo and emissivity, J. Geophys. Res.,
703 109, D21201, doi:10.1029/2004JD004945, 2004.
704
705 Johnson, B. T., Shine, K. P., and Forster, P. M.: The semi-direct aerosol effect:
706 Impact of absorbing aerosols on marine stratocumulus, Q. J. Roy. Meteor. Soc.,
707 130, 1407–1422, doi:10.1256/qj.03.61, 2004.
708
709 Koch, D. and Del Genio, A. D.: Black carbon semi-direct effects on cloud cover:
710 review and synthesis, Atmos. Chem. Phys., 10, 7685-7696,
711 doi:10.5194/acp-10-7685-2010, 2010.
712
713 Koren, I., Kaufman, Y. J., Remer, L. A., and Martins, J. V.: Measurement of the effect
714 of Amazon smoke on inhibition of cloud formation, Science, 303, 1342–1345, doi:
715 10.1126/science.1089424, 2004.
716
717 Kvalevåg, M. M., Samset, B. H., and Myhre, G.: Hydrological sensitivity to
718 greenhouse gases and aerosols in a global climate model, Geophys. Res. Lett.,
719 40, 1432–1438, doi:10.1002/grl.50318, 2013.
720
721 Liu, X., Ma, P.-L., Wang, H., Tilmes, S., Singh, B., Easter, R. C., Ghan, S. J., and
722 Rasch, P. J.: Description and evaluation of a new four-mode version of the Modal
723 Aerosol Module (MAM4) within version 5.3 of the Community Atmosphere Model,
724 Geosci. Model Dev., 9, 505–522, doi:10.5194/gmd-9-505-2016, 2016.
725
726 McFarquhar, G. M., Ghan, S., Verlinde, J., Korolev, A., Strapp, J. W., Schmid, B.,
727 Tomlinson, J. M., Wolde, M., Brooks, S. D., Cziczo, D., Dubey, M. K., Fan, J.,
728 Flynn, C., Gultepe, I., Hubbe, J., Gilles, M. K., Laskin, A., Lawson, P., Leaitch, W.
729 R., Liu, P., Liu, X., Lubin, D., Mazzoleni, C., Macdonald, A.-M., Moffet, R. C.,
730 Morrison, H., Ovchinnikov, M., Shupe, M. D., Turner, D. D., Xie, S., Zelenyuk, A.,
731 Bae, K., Freer, M., and Glen, A.: Indirect and Semi-Direct Aerosol Campaign
732 (ISDAC): The Impact of Arctic Aerosols on Clouds, B. Am. Meteorol. Soc., 92,
733 183–201, doi:10.1175/2010BAMS2935.1, 2011.

McFarquhar, G. M. and Wang, H.: Effects of Aerosols on Trade Wind Cumuli over the Indian Ocean: Model Simulations, Q. J. R. Meteorol. Soc., 132, 821–843, doi:10.1256/qj.04.179, 2006.

Meinshausen, M., Smith, S. J., Calvin, K., Daniel, J. S., Kainuma, M. L. T., Lamarque, J.-F., Matsumoto, K., Montzka, S. A., Raper, S. C. B., Riahi, K., Thomson, A., Velders, G. J. M., and van Vuuren, D. P. P.: The RCP greenhouse gas concentrations and their extensions from 1765 to 2300, Climatic Change, 109, 213–241, doi:10.1007/s10584-011-0156-z, 2011.

Ming, Y., Ramaswamy, V., and Persad, G.: Two opposing effects of absorbing aerosols on global-mean precipitation, Geophys. Res. Lett., 37, L13701, doi:10.1029/2010GL042895, 2010.

Morrison, H. and Gettelman, A.: A new two-moment bulk stratiform cloud microphysics scheme in the Community Atmosphere Model, version 3 (CAM3), Part I: Description and numerical tests, J. Clim., 21, 3642–3659, doi:10.1175/2008JCLI2105.1, 2008.

Oshima, N., Koike, M., Zhang, Y., Kondo, Y., Moteki, N., Takegawa, N., and Miyazaki, Y.: Aging of black carbon in outflow from anthropogenic sources using a mixing state resolved model: Model development and evaluation, J. Geophys. Res., 114, D06210, doi: 10.1029/2008JD010680, 2009.

Qian, Y., Wang, H., Zhang, R., Flanner, M. G., and Rasch, P. J.: A sensitivity study on modeling black carbon in snow and its radiative forcing over the Arctic and Northern China, Environ. Res. Lett., 9, 064001, doi:10.1088/1748-9326/9/6/064001, 2014.

Ramanathan, V. and Carmichael, G.: Global and regional climate changes due to black carbon, Nat. Geosci., 1, 221–227, doi:10.1038/ngeo156, 2008.

Sand, M., Berntsen, T. K., Kay, J. E., Lamarque, J. F., Seland, Ø., and Kirkevåg, A.: The Arctic response to remote and local forcing of black carbon, Atmos. Chem. Phys., 13, 211-224, doi:10.5194/acp-13-211-2013, 2013a.

Sand, M., Berntsen, T. K., Seland, Ø., and Kristjánsson, J. E.: Arctic surface temperature change to emissions of black carbon within Arctic or midlatitudes, J. Geophys. Res. Atmos., 118, 7788–7798, doi:10.1002/jgrd.50613, 2013b.

Sand, M., Iversen, T., Bohlinger, P., Kirkevåg, A., Seierstad, I., Seland, Ø., and Sorteberg, A: A standardized global climate model study showing unique

properties for the climate response to black carbon aerosols, J. Climate., 28, 2512–2526, doi:10.1175/JCLI-D-14-00050.1, 2015.

Sand, M., Berntsen, T. K., von Salzen, K., Flanner, M. G., Langner, J., and Victor, D. G.: Response of Arctic temperature to changes in emissions of short-lived climate forcers, Nat. Clim. Change, 6, 286–289, doi:10.1038/nclimate2880, 2016.

Shindell, D.: Inhomogeneous forcing and transient climate sensitivity, Nat. Clim. Change, 4, 274–277, doi:10.1038/nclimate2136, 2014.

Shindell, D. and Faluvegi, G.: Climate response to regional radiative forcing during the twentieth century, Nat. Geosci., 2, 294–300, doi:10.1038/ngeo473, 2009.

Shindell, D., Kuylenstierna, J. C. I., Vignati, E., van Dingenen, R., Amann, M., Klimont, Z., Anenberg, S. C., Muller, N., Janssens-Maenhout, G., Raes, F., Schwartz, J., Faluvegi, G., Pozzoli, L., Kupiainen, K., Höglund-Isaksson, L., Emberson, L., Streets, D., Ramanathan, V., Hicks, K., Oanh, N. T. K., Milly, G., Williams, M., Demkine, V., and Fowler, D.: Simultaneously Mitigating Near-Term Climate Change and Improving Human Health and Food Security, Science, 335, 183–189, doi:10.1126/science.1210026, 2012.

Smith, S. J. and Mizrahi, A.: Near-term climate mitigation by short-lived forcers, Proc. Natl. Acad. Sci., 110, 14202–14206, doi:10.1073/pnas.1308470110, 2013.

Stjern, C. W., Samset, B. H., Myhre, G., Forster, P. M., Hodnebrog, Ø., Andrews, T., Boucher, O., Faluvegi, G., Iversen, T., Kasoar, M., Kharin, V., Kirkevåg, A., Lamarque, J.-F., Olivieì, D., Richardson, T., Shawki, D., Shindell, D., Smith, C., Takemura, T., and Voulgarakis, A.: Rapid adjustments cause weak surface temperature response to increased black carbon concentrations, J. Geophys. Res. Atmos., 122, 11462–11481, doi:10.1002/2017JD027326, 2017.

Stohl, A., Aamaas, B., Amann, M., Baker, L. H., Bellouin, N., Berntsen, T. K., Boucher, O., Cherian, R., Collins, W., Daskalakis, N., Dusinska, M., Eckhardt, S., Fuglestvedt, J. S., Harju, M., Heyes, C., Hodnebrog, Ø., Hao, J., Im, U., Kanakidou, M., Klimont, Z., Kupiainen, K., Law, K. S., Lund, M. T., Maas, R., MacIntosh, C. R., Myhre, G., Myriokefalitakis, S., Olivié, D., Quaas, J., Quennehen, B., Raut, J.-C., Rumbold, S. T., Samset, B. H., Schulz, M., Seland, Ø., Shine, K. P., Skeie, R. B., Wang, S., Yttri, K. E., and Zhu, T.: Evaluating the climate and air quality impacts of short-lived pollutants, Atmos. Chem. Phys., 15, 10529–10566, doi:10.5194/acp-15-10529-2015, 2015.

Stohl, A., Klimont, Z., Eckhardt, S., Kupiainen, K., Shevchenko, V. P., Kopeikin, V. M., and Novigatsky, A. N.: Black carbon in the Arctic: the underestimated role of gas

820 flaring and residential combustion emissions, Atmos. Chem. Phys., 13, 8833–
821 8855, doi:10.5194/acp-13-8833-2013, 2013.
822
823 van Marle, M. J. E., Kloster, S., Magi, B. I., Marlon, J. R., Daniau, A.-L., Field, R. D.,
824 Arneth, A., Forrest, M., Hantson, S., Kehrwald, N. M., Knorr, W., Lasslop, G., Li,
825 F., Mangeon, S., Yue, C., Kaiser, J. W., and van der Werf, G. R.: Historic global
826 biomass burning emissions for CMIP6 (BB4CMIP) based on merging satellite
827 observations with proxies and fire models (1750–2015), Geosci. Model Dev., 10,
828 3329–3357, doi:10.5194/gmd-10-3329-2017, 2017.
829
830 Wang, H., Easter, R. C., Rasch, P. J., Wang, M., Liu, X., Ghan, S. J., Qian, Y., Yoon,
831 J.-H., Ma, P.-L., and Vinoj, V.: Sensitivity of remote aerosol distributions to
832 representation of cloud–aerosol interactions in a global climate model, Geosci.
833 Model Dev., 6, 765-782, doi:10.5194/gmd-6-765-2013, 2013.
834
835 Wang, M., Larson, V., Ghan, S., Ovchinnikov, M., Schanen, D., Xiao, H., Liu, X., Guo,
836 Z., and Rasch, P.: A multiscale modeling framework model (superparameterized
837 CAM5) with a higher-order turbulence closure: Model description and low-cloud
838 simulations, J. Adv. Model. Earth Syst., 7, 484–509, doi:10.1002/2014MS000375,
839 2015.
840
841 Yang, Y., Russell, L. M., Xu, L., Lou, S., Lamjiri, M. A., Somerville, R. C. J., Miller, A.
842 J., Cayan, D. R., DeFlorio, M. J., Ghan, S. J., Liu, Y., Singh, B., Wang, H., Yoon,
843 J.-H., and Rasch, P. J.: Impacts of ENSO events on cloud radiative effects in
844 preindustrial conditions: Changes in cloud fraction and their dependence on
845 interactive aerosol emissions and concentrations, J. Geophys. Res. Atmos., 121,
846 6321–6335, doi:10.1002/2015JD024503, 2016a.
847
848 Yang, Y., Russell, L. M., Lou, S., Lamjiri, M. A., Liu, Y., Singh, B., and Ghan, S. J.:
849 Changes in Sea Salt Emissions Enhance ENSO Variability, J. Climate, 29, 8575–
850 8588, doi:10.1175/JCLI-D-16-0237.1, 2016b.
851
852 Yang, Y., Wang, H., Smith, S. J., Ma, P.-L., and Rasch, P. J.: Source attribution of
853 black carbon and its direct radiative forcing in China, Atmos. Chem. Phys., 17,
854 4319-4336, doi:10.5194/acp-17-4319-2017, 2017.
855
856 Yang, Y., Wang, H., Smith, S. J., Zhang, R., Lou, S., Qian, Y., Ma, P.-L., Rasch, P. J.:
857 Recent intensification of winter haze in China linked to foreign emissions and
858 meteorology, Sci. Rep., 8, 2107, doi:10.1038/s41598-018-20437-7, 2018a.
859
860 Yang, Y., Wang, H., Smith, S. J., Zhang, R., Lou, S., Yu, H., Li, C., and Rasch, P. J.:
861 Source apportionments of aerosols and their direct radiative forcing and
862 long-term trends over continental United States, Earth's Future, 6, 793–808,
863 doi:10.1029/2018EF000859, 2018b.

Yang, Y., Wang, H., Smith, S. J., Easter, R. C., and Rasch, P. J.: Sulfate aerosol in the Arctic: Source attribution and radiative forcing, J. Geophys. Res. Atmos., 123, 1899–1918, doi:10.1002/2017JD027298, 2018c.

Zhang, R., Wang, H., Hegg, D. A., Qian, Y., Doherty, S. J., Dang, C., Ma, P.-L., Rasch, P. J., and Fu, Q.: Quantifying sources of black carbon in western North America using observationally based analysis and an emission tagging technique in the Community Atmosphere Model, Atmos. Chem. Phys., 15, 12805-12822, doi:10.5194/acp-15-12805-2015, 2015a.

Zhang, R., Wang, H., Qian, Y., Rasch, P. J., Easter, R. C., Ma, P.-L., Singh, B., Huang, J., and Fu, Q.: Quantifying sources, transport, deposition, and radiative forcing of black carbon over the Himalayas and Tibetan Plateau, Atmos. Chem. Phys., 15, 6205-6223, doi:10.5194/acp-15-6205-2015, 2015b.

Table 1. Changes in black carbon (BC) column burden, direct radiative effect (DRE) and cloud radiative effect (CRE) at the top of the atmosphere (TOA), surface BC snow/ice-albedo forcing, surface temperature (T) and total precipitation rate (P, including rain and snow) averaged over the Arctic (60–90°N), mid-latitudes (28–60°N) and the globe between perturbed (ARC150X/MID7X) and PD simulations. BC burden, DRE, CRE, and snow/ice-albedo forcing efficiencies, T sensitivity and P sensitivity are calculated as changes in regional mean BC column burden, DRE, CRE, snow/ice-albedo forcing, T and P divided by changes in global total BC emissions between perturbed and PD simulations, respectively. 1-σ for 80-annual means is shown in the parentheses. Note that these quantities include the impact of slow responses and feedbacks (e.g., changes in sea surface temperature and sea ice and feedbacks with clouds) so are not strictly comparable to the conventional definition of radiative forcing.

	ΔColumn Burden (mg m^{-2})			Burden Eff. (mg m^{-2} (Tg yr^{-1})$^{-1}$)			ΔDRE (W m^{-2})		
	60–90°N	28–60°N	Global	60–90°N	28–60°N	Global	60–90°N	28–60°N	Global
ARC150X	5.37 (±0.30)	1.34 (±0.05)	0.63 (±0.03)	0.425 (±0.024)	0.106 (±0.004)	0.050 (±0.002)	3.94 (±0.39)	0.83 (±0.04)	0.45 (±0.03)
MID7X	2.19 (±0.09)	3.97 (±0.09)	1.26 (±0.03)	0.106 (±0.004)	0.191 (±0.004)	0.061 (±0.001)	2.90 (±0.19)	2.49 (±0.09)	1.00 (±0.04)
	DRE Eff. (W m^{-2} (Tg yr^{-1})$^{-1}$)			ΔCRE (W m^{-2})			CRE Eff. (W m^{-2} (Tg yr^{-1})$^{-1}$)		
	60–90°N	28–60°N	Global	60–90°N	28–60°N	Global	60–90°N	28–60°N	Global
ARC150X	0.39 (±0.03)	0.11 (±0.00)	0.05 (±0.00)	–3.83 (±0.98)	–0.46 (±0.84)	–0.22 (±0.54)	–0.30 (±0.08)	–0.04 (±0.07)	–0.02 (±0.04)
MID7X	0.17 (±0.01)	0.22 (±0.01)	0.08 (±0.00)	–2.30 (±0.96)	–3.16 (±0.90)	–1.26 (±0.51)	–0.11 (±0.05)	–0.15 (±0.04)	–0.06 (±0.02)
	ΔSnow/ice-albedo Forcing (W m^{-2})			Snow/ice-albedo Eff. (W m^{-2} (Tg yr^{-1})$^{-1}$)			ΔT (K)		
	60–90°N	28–60°N	Global	60–90°N	28–60°N	Global	60–90°N	28–60°N	Global
ARC150X	1.26 (±0.08)	0.12 (±0.02)	0.10 (±0.01)	0.099 (±0.006)	0.010 (±0.002)	0.008 (±0.001)	2.13 (±0.65)	0.78 (±0.22)	0.48 (±0.26)
MID7X	0.53 (±0.05)	0.18 (±0.03)	0.07 (±0.01)	0.026 (±0.002)	0.009 (±0.001)	0.003 (±0.000)	0.48 (±0.79)	0.45 (±0.27)	0.23 (±0.26)
	T Sensitivity (K (Tg yr^{-1})$^{-1}$)			ΔP (mm day^{-1})			P Sensitivity (μm day^{-1} (Tg yr^{-1})$^{-1}$)		
	60–90°N	28–60°N	Global	60–90°N	28–60°N	Global	60–90°N	28–60°N	Global
ARC150X	0.169 (±0.052)	0.062 (±0.018)	0.038 (±0.020)	–0.043 (±0.079)	–0.011 (±0.066)	0.010 (±0.023)	–3.38 (±6.29)	–0.86 (±5.26)	0.77 (±1.84)
MID7X	0.023 (±0.038)	0.022 (±0.013)	0.011 (±0.012)	0.048 (±0.096)	–0.159 (±0.069)	–0.032 (±0.022)	2.34 (±4.61)	–7.67 (±3.34)	–1.52 (±1.04)

Table 2. BC burden, DRE, CRE, and snow/ice-albedo forcing efficiencies, T sensitivity and P sensitivity over the Arctic (60–90°N), mid-latitudes (28–60°N) and the globe between perturbed (ARC75X/ARC150X/MID3.5X/MID7X/MID14X) and PD simulations. 1-σ for 80-annual means is shown in the parentheses. Bold values between two simulations (ARC75X/ARC150X, MID3.5X/MID7X, and MID7X/MID14X) indicates statistically significant changes with 95% confidence from a two-tailed Student's t test.

		ARC75X	ARC150X			MID3P5X	MID7X	MID14X
		Burden Eff. (mg m^{-2} (Tg yr^{-1}) $^{-1}$)						
60–90°N		**0.406 (±0.021)**	**0.425 (±0.024)**			**0.095 (±0.005)**	**0.106 (±0.004)**	**0.124 (±0.004)**
28–60°N		**0.097 (±0.004)**	**0.106 (±0.004)**			**0.175 (±0.005)**	**0.191 (±0.004)**	**0.219 (±0.005)**
Global		**0.047 (±0.002)**	**0.050 (±0.002)**			**0.055 (±0.001)**	**0.061 (±0.001)**	**0.070 (±0.002)**
		DRE Eff. (W m^{-2} (Tg yr^{-1}) $^{-1}$)						
60–90°N		**0.346 (±0.036)**	**0.312 (±0.031)**			**0.146 (±0.014)**	**0.140 (±0.009)**	**0.137 (±0.006)**
28–60°N		**0.069 (±0.005)**	**0.066 (±0.003)**			**0.129 (±0.006)**	**0.120 (±0.004)**	**0.112 (±0.003)**
Global		**0.038 (±0.003)**	**0.035 (±0.003)**			**0.051 (±0.003)**	**0.048 (±0.002)**	**0.046 (±0.001)**
		CRE Eff. (W m^{-2} (Tg yr^{-1}) $^{-1}$)						
60–90°N		**–0.533 (±0.232)**	**–0.303 (±0.078)**			–0.091 (±0.166)	**–0.111 (±0.046)**	**–0.015 (±0.029)**
28–60°N		0.010 (±0.222)	–0.037 (±0.067)			**0.070 (±0.203)**	**–0.152 (±0.043)**	**0.129 (±0.035)**
Global		**–0.028 (±0.071)**	**–0.017 (±0.043)**			0.013 (±0.058)	**–0.061 (±0.025)**	**0.035 (±0.010)**
		Snow/ice-albedo Eff. (W m^{-2} (Tg yr^{-1}) $^{-1}$)						
60–90°N		**0.151 (±0.011)**	**0.099 (±0.006)**			**0.030 (±0.003)**	**0.026 (±0.002)**	**0.020 (±0.002)**
28–60°N		**0.013 (±0.003)**	**0.010 (±0.002)**			**0.011 (±0.002)**	**0.009 (±0.001)**	**0.007 (±0.001)**
Global		**0.012 (±0.001)**	**0.008 (±0.001)**			**0.004 (±0.001)**	**0.003 (±0.000)**	**0.003 (±0.000)**
		T Sensitivity (K (Tg yr^{-1}) $^{-1}$)						
60–90°N		**0.239 (±0.116)**	**0.169 (±0.052)**			0.042 (±0.098)	**0.023 (±0.038)**	**0.008 (±0.015)**
28–60°N		0.067 (±0.032)	0.062 (±0.018)			0.020 (±0.025)	**0.022 (±0.013)**	**0.015 (±0.005)**
Global		**0.040 (±0.035)**	**0.038 (±0.020)**			0.008 (±0.033)	**0.011 (±0.012)**	**0.005 (±0.005)**
		P Sensitivity (μm day-1 (Tg yr^{-1}) $^{-1}$)						
60–90°N		–2.88 (±13.39)	–3.38 (±6.29)			1.73 (±10.85)	2.34 (±4.61)	1.86 (±2.06)
28–60°N		–0.96 (±9.45)	–0.86 (±5.26)			–7.69 (±8.90)	**–7.67 (±3.34)**	**–8.53 (±1.61)**
Global		0.31 (±3.10)	0.77 (±1.84)			–1.99 (±2.81)	–1.52 (±1.04)	–2.15 (±0.49)

Figures for Paper

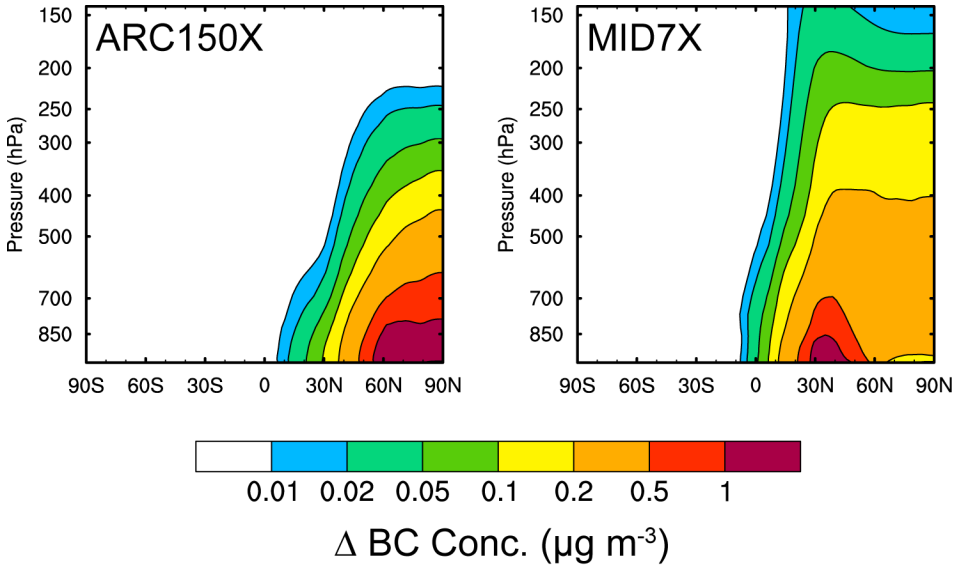

Figure 1. Difference in annual and zonal mean BC concentrations (μg m^{-3}) between ARC150X (left)/MID7X (right) and PD simulations.

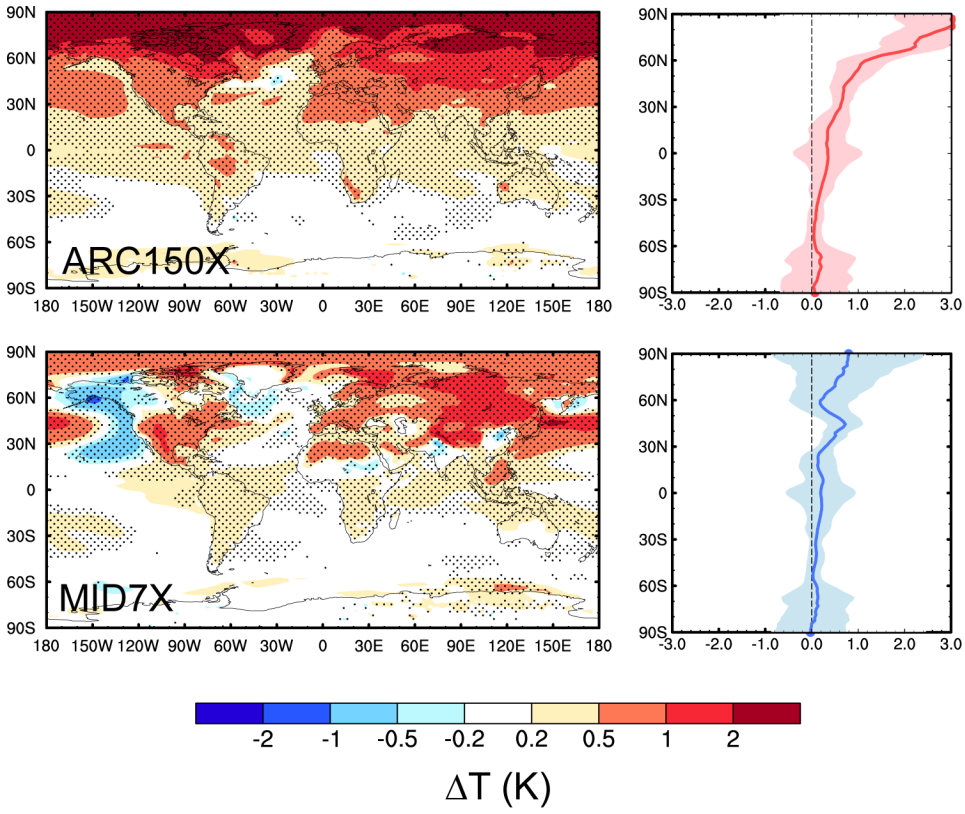

Figure 2. Spatial distribution (left) and zonal mean (right) of changes in annual mean surface air temperature (K) for ARC150X (top) and MID7X (bottom) compared to PD. The dotted areas in left panels indicate statistical significance with 95% confidence from a two-tailed Student's t test.

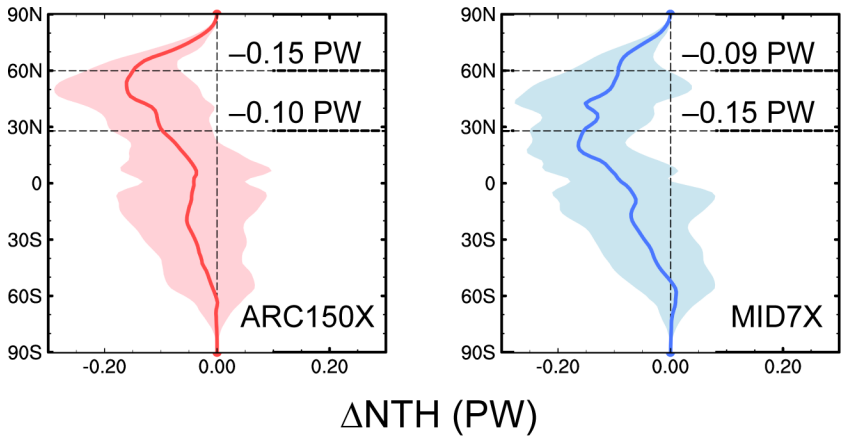

Figure 3. Zonal mean of changes in annual mean northward heat transport (NHT, PW) for ARC150X (left) and MID7X (right) compared to PD. Values of changes in NHT across 60°N and 28°N are shown in each panel. The shaded areas represent 1-σ for 80-annual means.

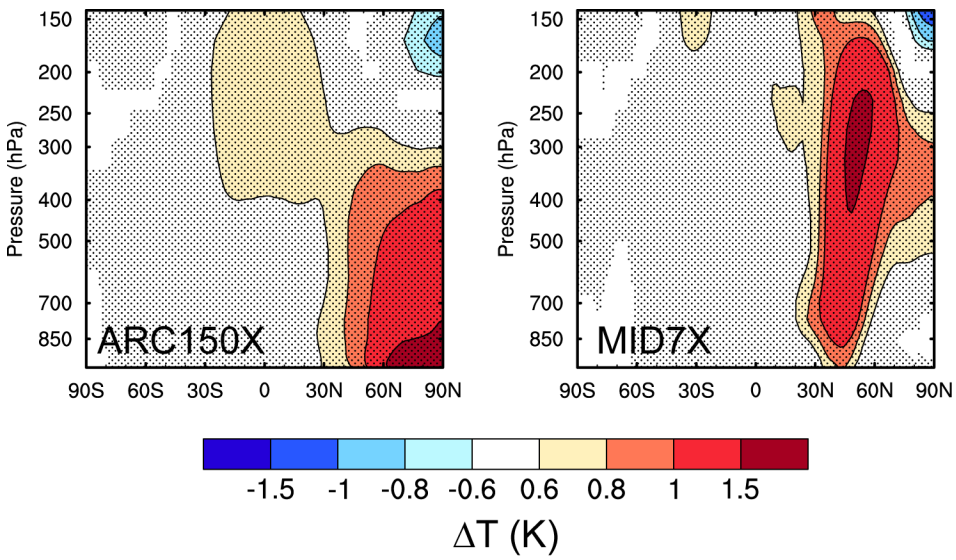

933

934

935 **Figure 4.** Changes in annual and zonal mean temperature (K) for ARC150X (left) and
936 MID7X (right) compared to PD. The dotted areas indicate statistical significance with
937 95% confidence from a two-tailed Student's t test.

938

939

940

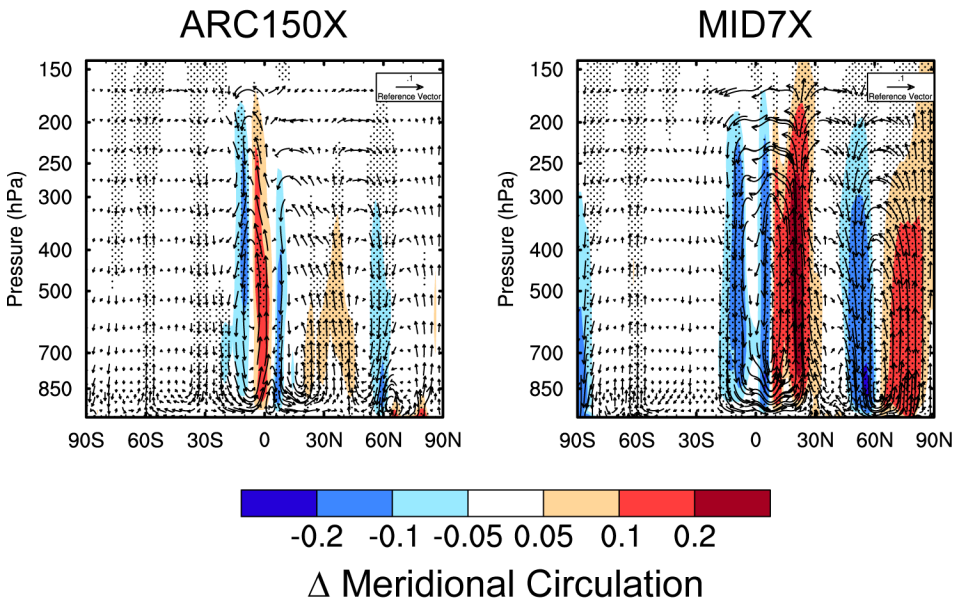

941
942
943 **Figure 5.** Changes in annual and zonal mean meridional wind vectors (m s^{-1}) and
944 vertical velocity (contours; Pa s^{-1} scaled by a factor of –100) for ARC150X (left) and
945 MID7X (right) compared to PD. The dotted areas indicate statistical significance with
946 95% confidence from a two-tailed Student's t test.
947
948

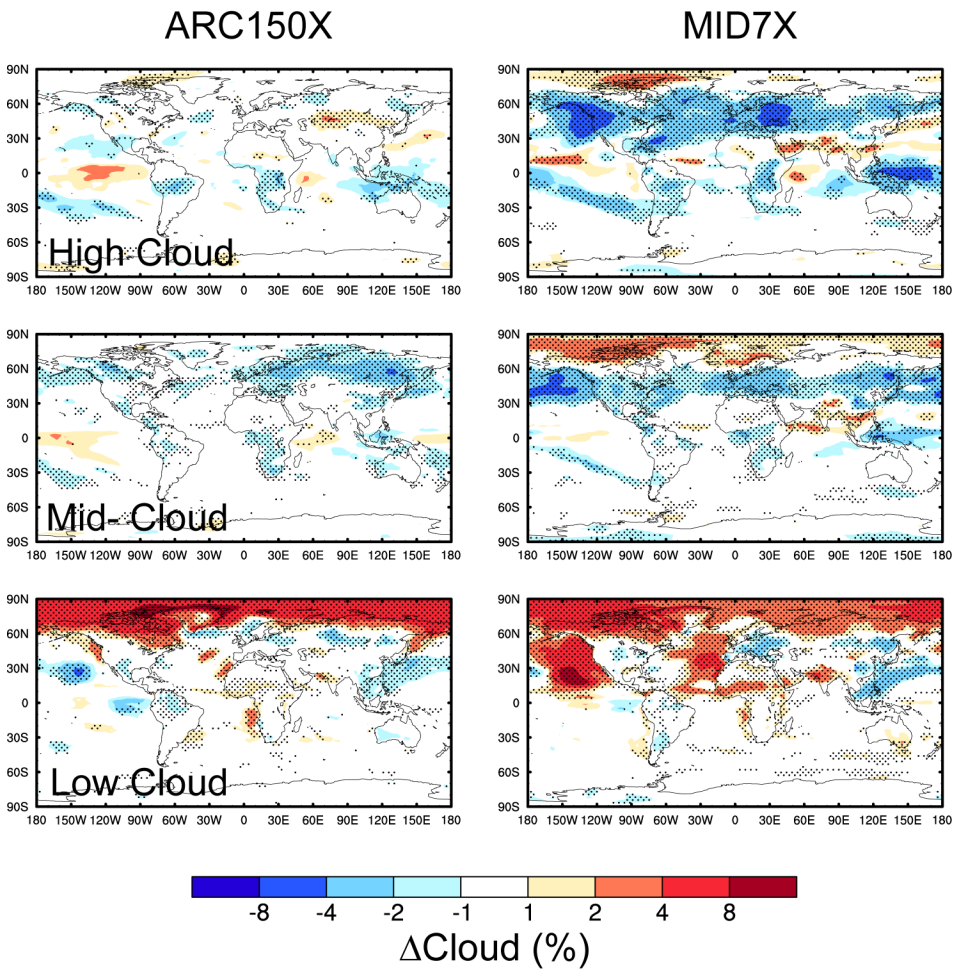

Figure 6. Changes in annual mean high (top), mid-level (middle), and low (bottom) cloud fraction (%) for ARC150X (left) and MID7X (right) compared to PD. The dotted areas indicate statistical significance with 95% confidence from a two-tailed Student's t test.

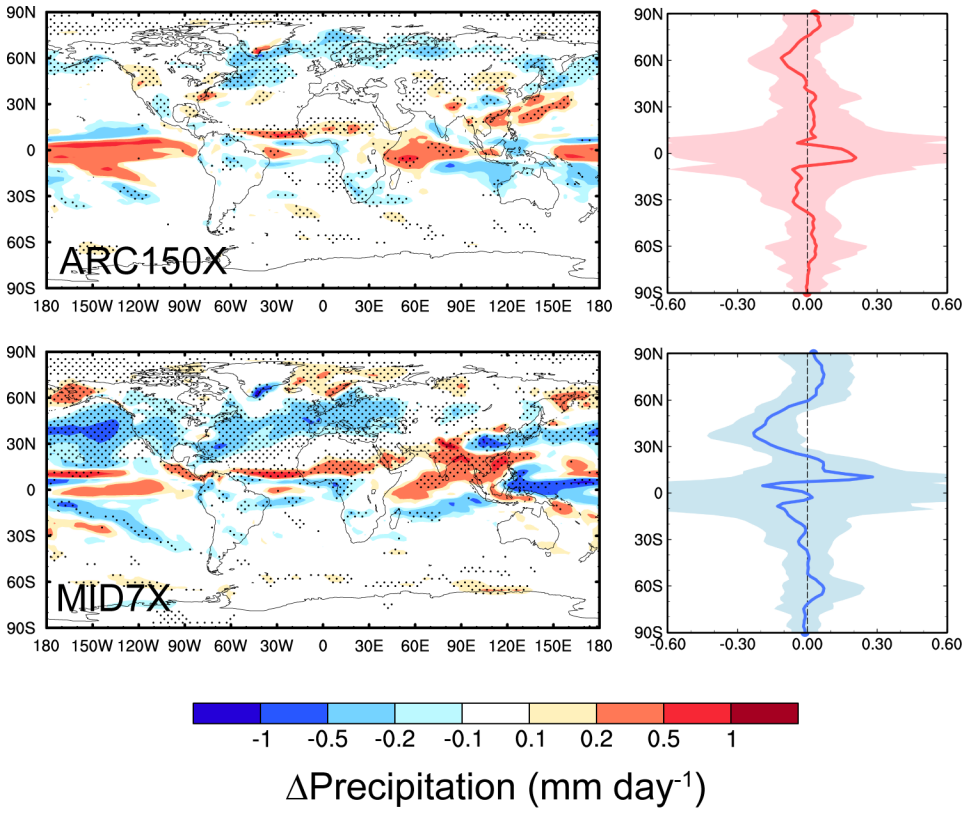

958
959
960 **Figure 7.** Spatial distribution (left) and zonal mean (right) of changes in annual mean
961 total precipitation rate (mm day^{-1}) for ARC150X (top) and MID7X (bottom) compared
962 to PD. The dotted areas in left panels indicate statistical significance with 95%
963 confidence from a two-tailed Student's t test.
964
965

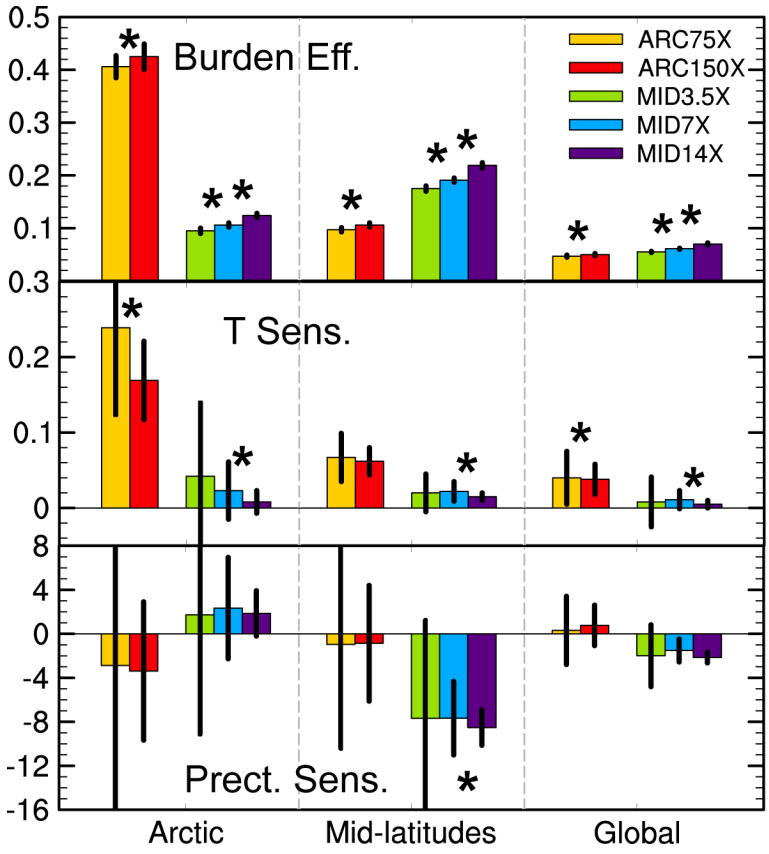

966

967

968 **Figure 8.** Burden efficiencies, temperature and precipitation sensitivities over the
969 Arctic, mid-latitudes and the whole globe for ARC75X, ARC150X, MID3.5X, MID7X
970 and MID14X. Burden efficiencies, temperature sensitivity and precipitation sensitivity
971 are calculated as changes in regional mean BC column burden, surface temperature
972 and total precipitation rate divided by changes in global total BC emissions between
973 perturbed and PD simulations, respectively. Error bars represent 1-σ for 80-annual
974 means. Asterisk between two bars (ARC75X/ARC150X, MID3.5X/MID7X, and
975 MID7X/MID14X) indicates statistically significant changes with 95% confidence from
976 a two-tailed Student's t test.

977

978

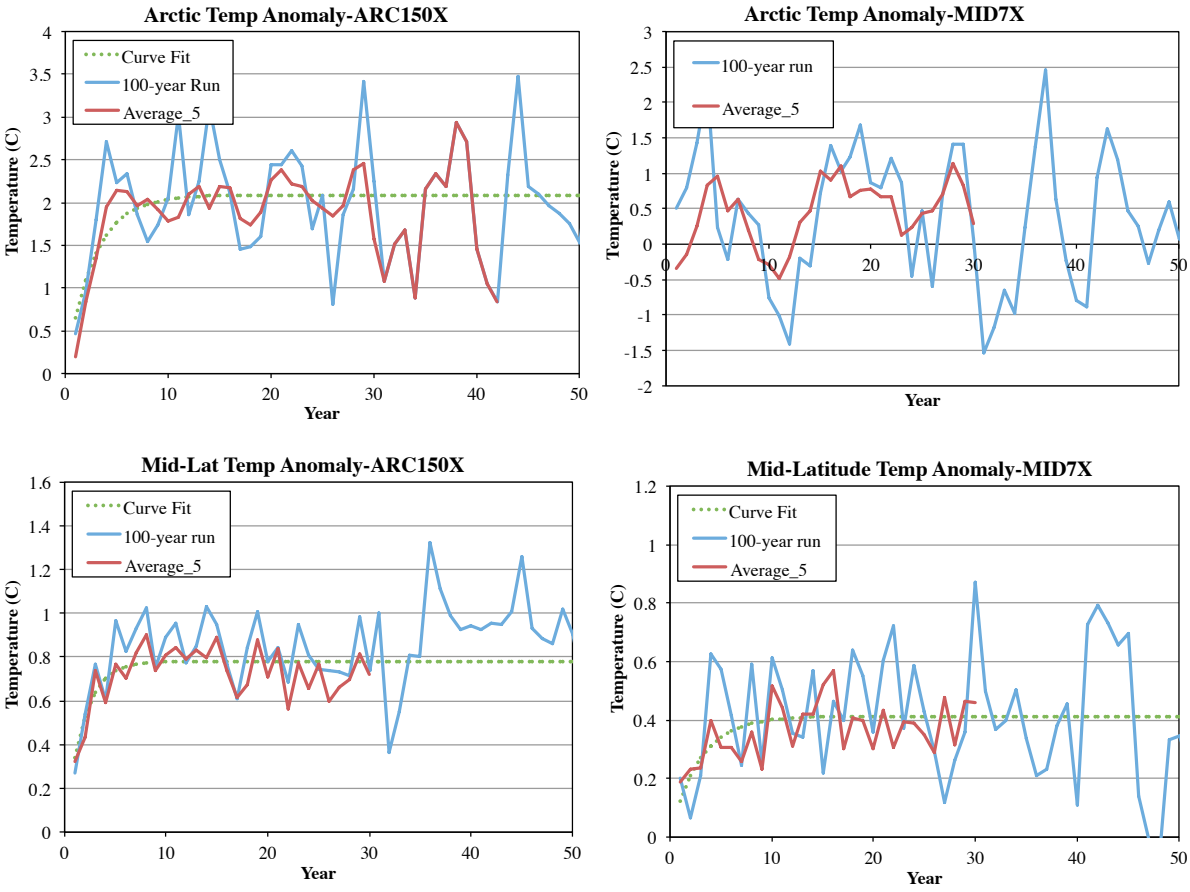

Figure 9. Time series of mean surface temperature response from ARC150X (left) and MID7X (right) BC emission perturbations as compared to PD. The response is shown over the Arctic (top) and mid-latitudes (bottom). Shown are the 100-year ensemble simulation (blue lines), the average of five 30-year ensemble members (red), and a numerical fit for an exponential approach to the long-term average (green dashed line). Curve fits used the package STAN in R, which is Bayesian inference using the No-U-Turn sampler. Note that MID7X Arctic temperature response does not result in a fit due to noise.

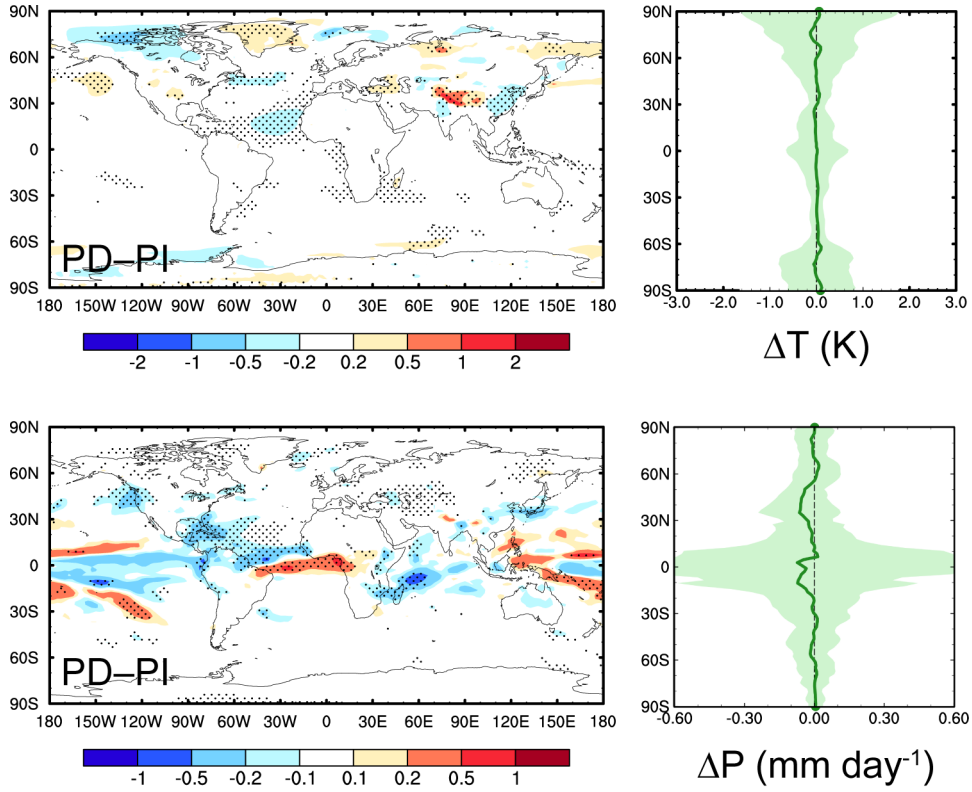

Figure 10. Spatial distribution (left) and zonal mean (right) of differences in annual mean surface temperature (K, top) and total precipitation rate (mm day^{-1}, bottom) between PD and PI. The dotted areas in left panels indicate statistical significance with 95% confidence from a two-tailed Student's t test.